Title

Essential role of RGS-PX1/sorting nexin 13 in mouse development and regulation of endocytosis dynamics

Journal

Proceedings of the National Academy of Sciences of the United States of America, 103(45)

ISSN

0027-8424

Authors

Zheng, Bin
Tang, Tingdong
Tang, Nan
et al.

Publication Date

2006-11-07

Peer reviewed

Essential role of RGS-PX1/sorting nexin 13 in mouse development and regulation of endocytosis dynamics

Bin Zheng*†, Tingdong Tang*, Nan Tang‡, Krystyna Kudlicka*, Kazuaki Ohtsubo*, Phuong Ma*, Jamey D. Marth*, Marilyn G. Farquhar*§, and Eero Lehtonen*¶

Departments of *Cellular and Molecular Medicine and ‡Biology, University of California at San Diego, La Jolla, CA 92093-0651

Contributed by Marilyn G. Farquhar, September 11, 2006

RGS-PX1 (also known as sorting nexin 13) is a member of both the regulator of G protein signaling (RGS) and sorting nexin (SNX) protein families. Biochemical and cell culture studies have shown that RGS-PX1/SNX13 attenuates Gαs-mediated signaling through its RGS domain and regulates endocytic trafficking and degradation of the epidermal growth factor receptor. To understand the functions of RGS-PX1/SNX13 *in vivo*, we generated mice carrying targeted mutations of *Snx13* and found that systemic *Snx13*-null mice were embryonic lethal around midgestation. *Snx13*-null embryos had significant overall growth retardation and defects in neural tube closure, blood vessel formation, and the formation of the placental labyrinthine layer. Moreover, the *Snx13*-null visceral yolk sac endoderm cells showed dramatic changes in the organization of endocytic compartments, abundant autophagic vacuoles, and abnormal localization of several endocytic markers, including megalin, a receptor for nutrients and proteins; ARH, a coat protein that binds megalin; LAMP2; and LC3. These changes suggest that *Snx13*-null embryos are defective in nutrient uptake and transport, which may contribute to the other developmental abnormalities observed. Taken together, our findings demonstrate an essential role for RGS-PX1/SNX13 in mouse development and provide previously undescribed insights into its cellular function in the regulation of endocytosis dynamics.

megalin | receptor endocytosis | regulator of G protein signaling | visceral yolk sac endoderm

Receptor-mediated endocytosis is the process by which plasma membrane components and extracellular materials such as nutrients, hormones, antigens, and other macromolecules are selectively internalized into cytoplasmic vesicles, delivered to early and late endosomes and degraded in lysosomes or recycled back to the plasma membrane through recycling endosomes (1–3). Trafficking between these endocytic compartments is highly regulated and often involves critical sorting steps. Recently, a large family of sorting nexin (SNX) proteins characterized by the presence of Phox (PX) domains has been identified and implicated in the regulation of different steps of the endocytic pathway (4, 5). For example, the founding member of the SNX family, SNX1, was identified as an interacting partner of the epidermal growth factor receptor, and overexpression of SNX1 was found to enhance lysosomal degradation of epidermal growth factor receptor (6). More recently, knock-down of SNX1 expression by RNA interference was shown to perturb the steady state distribution of the cation-independent mannose-6-phosphate receptor (CI-MPR) from the trans-Golgi network to endosomes and to increase the degradation rate of CI-MPR, establishing a role for SNX1 in endosome-to-trans-Golgi network transport (7).

RGS-PX1 (also known as SNX 13, the designation by the human gene nomenclature committee) was identified originally as a member of the regulator of G protein signaling (RGS) protein family through bioinformatics analysis (8). RGS-PX1 contains a characteristic RGS domain that specifically binds to the stimulatory subunit of the heterotrimeric G protein Gαs but not other Gα proteins (8, 9) and serves as a GTPase activating protein for Gαs (8). In addition, RGS-PX1/SNX13 also contains a PX domain that preferentially binds to phosphatidylinositol-3-phosphate which is enriched in early endosomes (8). We showed previously that RGS-PX1/SNX13 is localized in early endosomes, and overexpression of RGS-PX1/SNX13 delays the degradation of epidermal growth factor receptor, probably at the steps of endosome sorting and lysosomal targeting (8). More recently, we found that RGS-PX1 and Gαs form a complex with Hrs (hepatocyte growth factor-regulated tyrosine kinase substrate), a critical component of the endosomal sorting machinery that targets ubiquitinated membrane proteins for sequestration into multivesicular bodies and subsequent degradation in lysosomes (10). These studies using cultured mammalian cells demonstrated that RGS-PX1 plays an important role in the regulation of endocytic trafficking.

To understand the functions of RGS-PX1/SNX13 *in vivo*, we generated *Snx13*-deficient mice through homologous recombination in ES cells. We show that $Snx13^{-/-}$ embryos are growth retarded and die around midgestation. Mutant embryos also show defects in neural tube closure, vasculogenesis and placental development. Electron microscopy and immunofluorescence analysis revealed unusual prominent tubular endosomal compartments, presence of autophagic vacuoles, and redistribution of endosomal markers in mutant visceral yolk sac (VYS) endoderm. These results indicate that RGS-PX1/SNX13 plays important roles in embryo development and in the dynamics of endocytosis in VYS endoderm and provide insights into the role of RGS-PX1/SNX13 in receptor recycling and endosomal-lysosomal trafficking.

Results

Targeted Disruption of the Mouse *RGS-PX1*/*Snx13* Gene. To explore the function of RGS-PX1/SNX13 *in vivo*, we disrupted the mouse gene through homologous recombination in ES cells (Fig. 1*A–E*). A gene-targeting construct was assembled to allow the excision of coding exon 3 and removal of the marker genes by Cre recombinase that is expected to generate a translational frameshift mutation and a premature translation product containing only the N-terminal 42 residues of RGS-PX1. After electroporation and selection, ES cells were analyzed for homologous recombination by PCR and Southern blotting (Fig. 1*F*). ES cells containing the type I systemic deletion mutant were microinjected into C57BL/6 blastocysts to generate chimeric mice, which were bred with C57BL/6 mice to produce germ-line-transmitted $Snx13^{+/-}$ mice.

Author contributions: B.Z., M.G.F., and E.L. designed research; B.Z., T.T., N.T., K.K., P.M., and E.L. performed research; K.O. and J.D.M. contributed new reagents/analytic tools; B.Z., N.T., M.G.F., and E.L. analyzed data; and B.Z., M.G.F., and E.L. wrote the paper.

The authors declare no conflict of interest.

Abbreviations: E*n*, embryonic day *n*; PFA, paraformaldehyde; RGS, regulator of G protein signaling; SNX, sorting nexin; VYS, visceral yolk sac.

†Present address: Division of Signal Transduction, Beth Israel Deaconess Medical Center and Department of Systems Biology, Harvard Medical School, Boston, MA 02115.

§To whom correspondence should be addressed. E-mail: mfarquhar@ucsd.edu.

¶Present address: Department of Pathology, Haartman Institute, P.O. Box 21, 00014, University of Helsinki, FIN-00014, Helsinki, Finland.

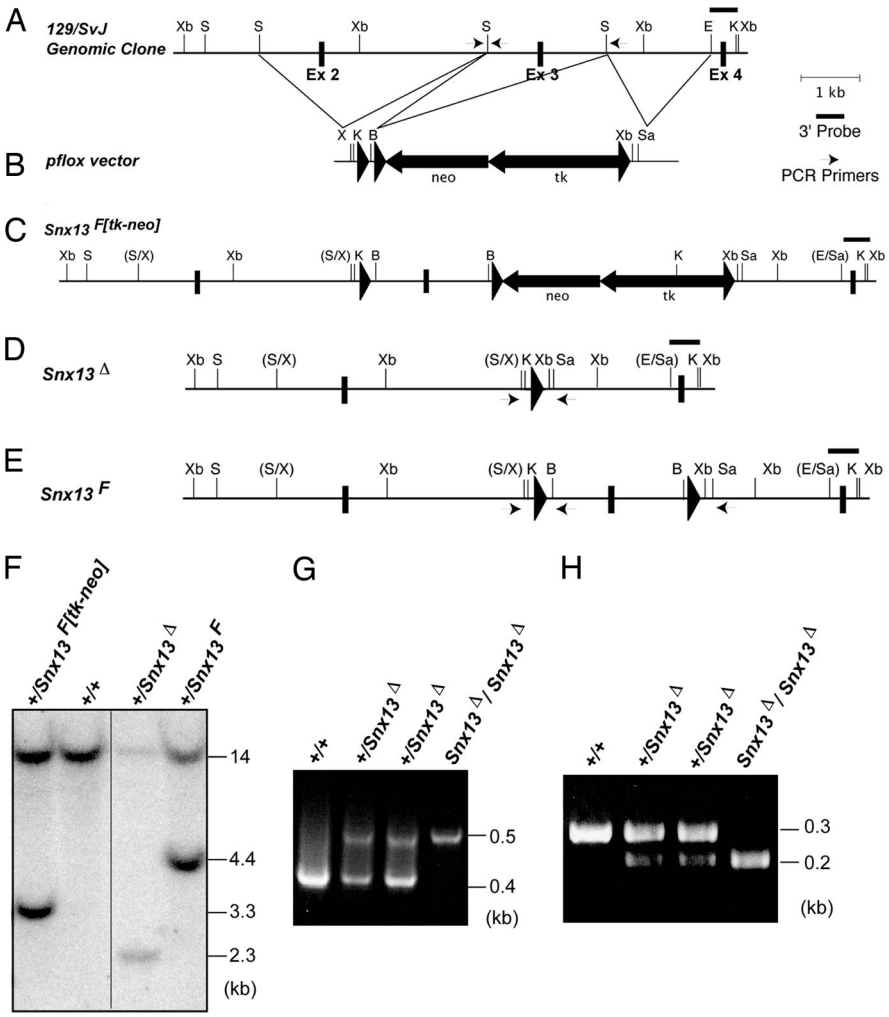

Fig. 1. Targeted disruption of the *Snx13* gene. (*A–E*) A mouse genomic clone of *Snx13* (*A*) was isolated and used in generating the targeting construct in pflox (*B*) as indicated. (*C*) Homologous recombination in ES cells produces the $Snx13^{F[tk–neo]}$ allele. (*D* and *E*) Transient expression of Cre recombination and ganciclovir selection generates ES subclones containing $Snx13^{\Delta}$ (systemic-null) (*D*) and $Snx13^{F}$ (conditional-null) (*E*) alleles. Black rectangles indicate coding exons; triangles indicate *loxP* sites. B, BamHI; E, EcoRV; K, KpnI; S, SphI; Sa, SalI; X, XhoI; Xb, XbaI. (*F*) Southern blotting analysis of ES cell DNAs containing wild-type, $Snx13^{F[tk-neo]}$, $Snx13^{\Delta}$, and $Snx13^{F}$ alleles. Genomic DNA was digested with KpnI and blotted with a radiolabeled 3′ probe as indicated in *A*. (*G*) PCR analysis of DNA extracted from visceral yolk sacs of wild-type (+/+), heterozygous (+/$Snx13^{\Delta}$), and homozygous ($Snx13^{\Delta}/Snx13^{\Delta}$) embryos by using primers indicated in *A* and in methods. (*H*) RT-PCR analysis showing the deletion of exon 3 from *Snx13* transcript in homozygous embryos. RNA was extracted from E10.5 embryos, and RT-PCR was performed by using primers corresponding to the boundary of exon 1/2 and the 3′ end of exon 4. Wild-type and mutant Snx13 transcripts generate fragments of 306 and 203 bp, respectively.

***Snx13*$^{-/-}$ Embryos Die at Midgestation.** Both Snx13 heterozygous male and female mice were fertile and did not show obvious phenotypic abnormalities by the age of 18 months. However, breeding of Snx13 heterozygous mice resulted in no homozygous mice at birth (Table 1), indicating that mice lacking SNX13 died during embryogenesis. To determine the time of embryonic death, embryos from timed matings between heterozygous mice were analyzed at different stages of gestation, and the genotypes of embryos were determined by PCR (Fig. 1*G*). Between embryonic day (E) 8.5 and E10.5, *Snx13*$^{-/-}$ embryos were found at the proper Mendelian ratio (Table 1). After E11.5, the number of viable mutant embryos decreased significantly (Table 1). No live homozygous mutant embryos were found after E14.5 (Table 1). A significant number of resorbing embryos and empty deciduas were also found from E10.5 to E13.5. RT-PCR performed on RNA isolated from homozygous *Snx13*$^{-/-}$ and wild-type embryos or VYS confirmed that the targeted exon 3 is not present in the mutant RNA (Fig. 1*H*).

Growth Retardation, Neural Tube Closure Defects and Impaired Vasculogenesis in *Snx13*$^{-/-}$ Embryos. Between E8.5 and E13.5, *Snx13*$^{-/-}$ embryos were significantly smaller than their wild-type littermates (Fig. 2*A*). Other than their small size, the most striking abnormality was that the *Snx13*$^{-/-}$ embryos frequently showed failure of neural tube closure. At E10.5–11.5, mutant embryos typically presented with everted, open cranial neural folds (Fig. 2 *A* and *C*). We also analyzed the vascularization in wild-type and *Snx13*$^{-/-}$ embryos by staining embryos for CD31 (PECAM-1), an endothelial marker. We found that the mutant mice (Fig. 2*C*) showed a distinctly abnormal cephalic vascularization, less arborized compared with their wild-type littermates (Fig. 2*B*). The number of capillaries was particularly small in the anterior (Fig. 2*C*) and posterior aspects of neural folds that had failed to close, and the general organization of the capillary network was quite irregular.

Placental Defects in *Snx13*$^{-/-}$ Embryos. We also analyzed the placentas of *Snx13*-null embryos around midgestation. At E10.5 the placentas of the *Snx13*$^{-/-}$ mice were grossly similar, and histologically there were no distinct differences from their wild-type littermates (data not shown). By E11.5–E13.5, the placentas of the mutant embryos (Fig. 2*E Inset*) were significantly smaller than those of their wild-type littermates (Fig. 2*D Inset*). At E11.5, the

Table 1. Genotype analysis of offspring from *Snx13* $^{+/-}$ crosses

Age	+/+ (*n*)	+/− (*n*)	−/− (*n*)	N/D
Postnatal	44	80	0	
E14.5–16.5	8	24(1)	0	
E12.5–13.5	9(2)	26(4)	8(3)	
E11.5	12	16	8(2)	3
E10.5	36(2)	65	37(2)	3
E8.5–9.5	12	22	7	4

n, number of embryos that were dead/resorbing; N/D, genotype could not be dertermined due to technical difficulties.

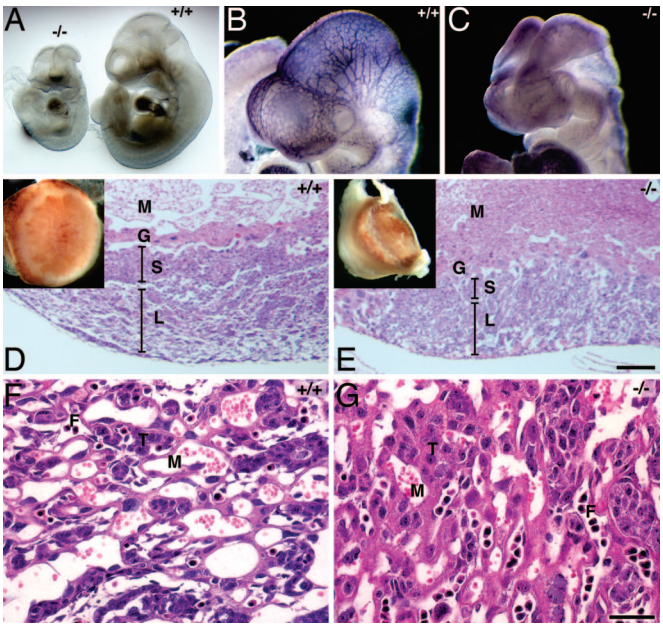

Fig. 2. *Snx13*-null embryos are smaller than their littermates and show defects in neural tube closure, vasculogenesis, and placental morphology. (*A*) E10.5 embryos. The *Snx13*-null embryo (*Left*) is considerably smaller than its littermate (*Right*) and has a neural tube closure defect. (*B*) Whole-mount staining for CD31 (PECAM-1) showing normal vascularization in the head of an E10.5 wild-type embryo. (*C*) Similar CD31 staining of *Snx13*-null littermate with a defect in cranial neural tube closure. Vascularization is particularly defective in the everted open neural tube. (*D* and *E*) Placentas of wild-type (*D*) and *Snx13*-null (*E*) embryos. The placenta of the *Snx13* mutant embryo appears smaller (*E Inset*) and more hypoplastic than that of the wild-type littermate. M, maternal decidua; G, giant trophoblast cell layer; S, syncytiotrophoblast layer; L, labyrinthine layer. (*F* and *G*) Labyrinth layer of placentas of wild-type (*F*) and *Snx13*-null (*G*) embryos. The wild-type labyrinthine layer shows normal syncytiotrophoblast differentiation and fetal and maternal vascularization. In the $Snx13^{-/-}$ labyrinth layer, the trophoblast cells (T) appear undifferentiated and are abnormally large and granular. The vascular spaces are reduced compared with the wild-type littermate. F, fetal blood vessel; M, maternal blood sinus; T, trophoblast. Placentas were fixed in neutral formalin. Paraffin sections were stained with hematoxylin and eosin. (Scale bars: *D* and *E*, 50 μm; *F* and *G*, 100 μm.)

giant cell and spongiotrophoblast layers appeared similar in the wild-type (Fig. 2*D*) and mutant (Fig. 2*E*) placentas. There were distinct abnormalities in the labyrinthine layer in the mutant placentas (Fig. 2 *F* and *G*). The $Snx13^{-/-}$ trophoblast cells had large nuclei and abundant granular cytoplasm, which often was more eosinophilic than that of the wild-type littermates. The apparent failure of labyrinthine trophoblast differentiation was accompanied by reduced maternal vascular spaces in the labyrinthine layer. The fetal blood supply appeared similar in both genotypes, but the $Snx13^{-/-}$ fetal labyrinthine vessels often appeared wider than the corresponding wild-type vessels (Fig. 2 *F* and *G*), suggesting a defect in branching morphogenesis. No clear changes were detected in the maternal decidua of the placentas at any stage studied. Taken together, these findings indicate that $Snx13^{-/-}$ embryos have defective development of the labyrinthine layer of the placenta.

Abnormal Endosomal Compartments and Presence of Autophagic Vacuoles in $Snx13^{-/-}$ Visceral Yolk Sac Endoderm. During midgestation, the VYS endoderm which is derived from the embryo is the major supplier of nutrients for the mouse conceptus (11, 12). The VYS endoderm cells are highly specialized for endocytosis and lysosomal degradation. Nutrients, such as proteins and vitamins taken up by endocytosis via the receptors megalin and cubilin (13), are processed in lysosomes and the resultant products are delivered

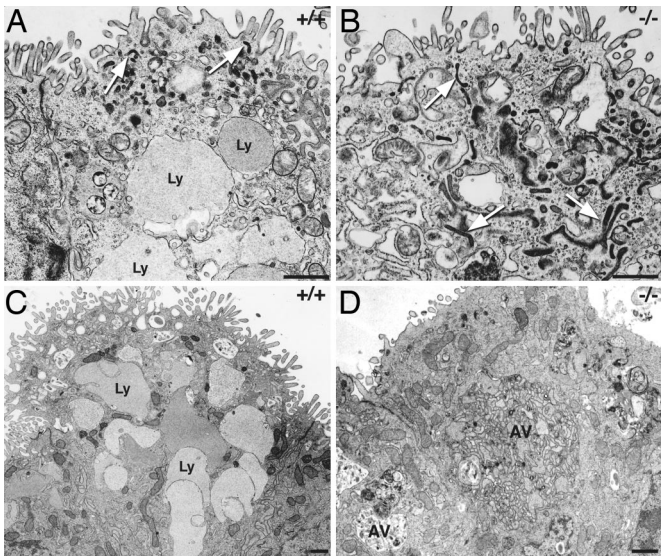

Fig. 3. Electron micrographs showing abnormal endosomal compartments and autophagic vacuoles in *Snx13*-null VYS endoderm cells. (*A*) At E10.5 wild-type VYS endoderm cells show small dense tubular structures (arrows) corresponding to apical endosomes and a collection of large lysosomal/endosomal vacuoles (Ly) with content of varying density. (*B*) In the null-mutant apical dense tubular endosomes (arrows) are more abundant and elaborate. (*C*) At E11.5, the wild-type VYS endoderm cells contain large, vacuolar lysosomes/endosomal (Ly) similar to those at E10.5. (*D*) The *Snx13*-null VYS endoderm cells contain numerous autophagic vacuoles (AV) with membranous residues inside. VYS samples were fixed in 1.5% glutaraldehyde, 3% PFA, and processed as described in *Materials and Methods*. Epon sections were stained with uranyl acetate and lead citrate. (Scale bars: 1 μm.)

to the embryo (14, 15). The abnormalities we observed in the mutant embryos, such as growth retardation and neural tube closure defects, could be related to functional defects in the VYS endoderm. To determine whether any morphological changes could be detected in the VYS endoderm we analyzed this cell layer from midgestation litters by electron microscopy. As shown in Fig. 3*A*, at E10.5 the wild-type VYS endoderm cells characteristically show abundant large vacuolar structures and smaller electron-dense tubular elements in their apical cytoplasm which represent components of the endosome/lysosomal system. In the $Snx13^{-/-}$ mutant VYS endoderm cells (Fig. 3*B*), the characteristic large apical vacuoles are smaller and less numerous, and the dense tubules are more abundant and more elaborate. The latter resemble the branching dense apical tubules found in the cells of the kidney proximal tubule that carry endosomal markers and have been identified as recycling endosomal tubules (16, 17).

At E11.5, the $Snx13^{-/-}$ VYS endoderm cells show numerous large autophagic vacuoles (Fig. 3*D*) that contain membranous residues not found in the VYS endoderm cells of the wild-type littermates (Fig. 3*C*). Autophagic vacuoles are readily recognizable by their content of membranous whorls and other structures (Fig. 3*D*). Autophagy represents a pathway for degradation of intracellular organelles and often occurs under pathologic conditions in which cells are stressed or lack proper nutrients (e.g., essential amino acids) (18). The presence of autophagic vacuoles in E11.5 mutant embryos suggested potential defects in nutrient uptake through receptor-mediated endocytosis and/or lysosomal degradation.

Redistribution of Endocytic Markers in $Snx13^{-/-}$ Mice. To further delineate the changes in the endosomal system we stained VYS for endocytic markers, including megalin (one of the main endocytic receptors of this epithelium), ARH (marker for coated vesicles and

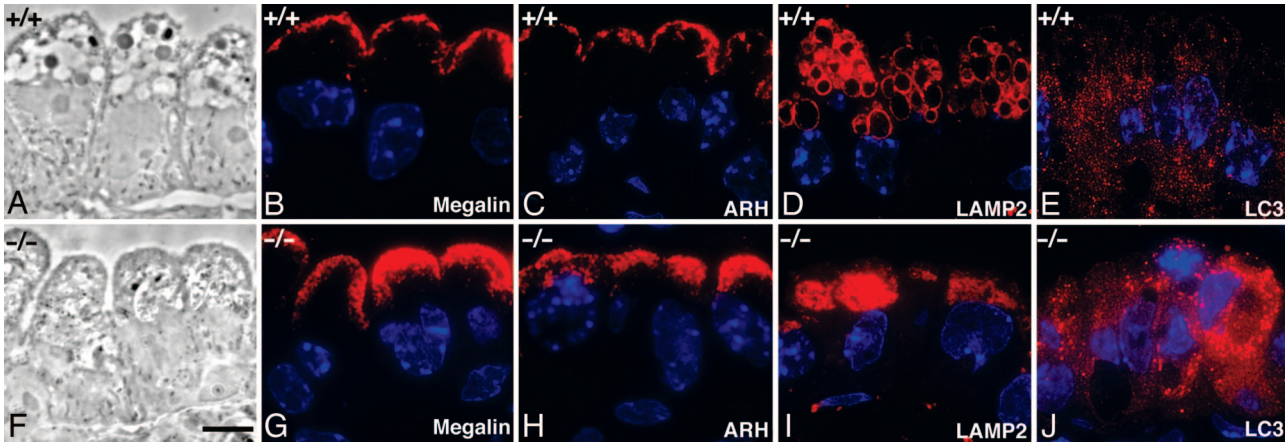

Fig. 4. Changes in the distribution of endocytic markers in *Snx13*$^{-/-}$ VYS endoderm. (*A*) By phase contrast microscopy of wild type E11.5 embryo, numerous vacuolated endosomes and lysosomes are seen in the apical cytoplasm between the cell nucleus and the apical cell membrane. (*B–E*) In wild-type VYS endoderm cells, megalin (*B*) and coat protein ARH (*C*) are mainly seen along the apical plasma membrane, most likely in clathrin-coated pits; the lysosomal marker LAMP2 (*D*), distributed in ring-like structures, represents the membranes of the large apical endosomes/lysosomes; and staining for the autophagy marker LC3 (*E*) is very weak and sparse. (*F–J*) In contrast, by phase-contrast microscopy of E11.5 *Snx13*$^{-/-}$ embryos (*F*), there are multiple vacuoles that appear smaller in size that those in wild-type embryos, and some most likely represent the autophagic vacuoles with heterogeneous contents seen by EM (Fig. 3). In a *Snx13*-null littermate, megalin (*G*) and ARH (*H*) are more broadly distributed in endosomal compartments in the apical cytoplasm; LAMP2 (*I*) is found in some large ring-like structures, as well as in the giant autophagic vacuoles; and LC3 (*J*) staining is greatly increased and widely distributed in punctate preautophagosomes located throughout the cytoplasm surrounding the autophagic vacuoles. Increased staining for LC3 is indicative of increased autophagy. VYS were fixed in 4% PFA, and semithin cryosections were prepared and stained as described in *Materials and Methods*. (Scale bar: 5 μm.)

endosomes) and LAMP2 (a lysosomal marker). Megalin continually internalizes multiple proteins, including vitamin carriers, delivers them to endocytic compartments and recycles to the cell surface (13, 19). Megalin is found throughout the endocytic system but at steady state is most concentrated in clathrin coated pits at the apical plasma membrane in the proximal kidney tubule, another epithelium involved in bulk endocytosis (17, 20). In semithin frozen sections of cells from E11.5 wild-type VYS endoderm cells, megalin is mainly seen immediately beneath the apical plasma membrane (Fig. 4*C*) where it codistributes with the coat proteins ARH (Fig. 4*C*) and clathrin (data not shown). In *Snx13*$^{-/-}$ littermates, both megalin (Fig. 4*G*) and ARH (Fig. 4*H*) have a much broader distribution in the apical cytoplasm, suggesting redistribution of megalin and ARH which escorts megalin to and through the apical tubular endosomal system (21). The distribution of LAMP2 in the wild-type VYS endoderm cells (Fig. 4*D*) coincided with the distribution of large cytoplasmic vacuoles with contents of varying density seen by phase contrast (Fig. 4*A*) and electron microscopy (Fig. 3 *A* and *C*). In the VYS of *Snx13*$^{-/-}$ mice (Fig. 4*I*), LAMP2 antibodies stained the apical cytoplasm between the nucleus and early endosomes, the region where the autophagic vacuoles are often seen by EM.

To check for the presence of autophagy we stained VYS for the autophagy marker, LC3. LC3 typically is located in the cytoplasm but becomes associated with small "preautophagosomes" that surround the large autophagic vacuoles on initiation of autophagy (22). Interestingly, *Snx13*$^{-/-}$ VYS cells showed numerous vesicles positive for LC3 surrounding the large autophagic vacuoles (Fig. 4*J*). LC3-positive vesicles were rarely seen in the corresponding wild-type cells (Fig. 4*E*). From these findings we conclude that in the VYS endoderm of wild-type embryos, vacuolated lysosomes are abundant reflecting the high levels of protein uptake, whereas in VYS endoderm cells of the *Snx13*$^{-/-}$ mice tubular endosomes are abundant, fewer lysosomes are seen, and autophagy is prominent.

Discussion

In this study we generated a mutant allele of mouse *Snx13* by gene targeting and demonstrated that RGS-PX1/SNX13 plays an essential role in mouse development. Disruption of the *Snx13* gene led to embryonic lethality around midgestation. Morphological and histological analyses revealed that mutant embryos showed overall growth retardation and defects in neural tube closure and vasculogenesis at earlier stages. It is interesting to note that homozygous disruption of the *Gnas* gene which encodes Gαs, the GTPase regulated by RGS-PX1/SNX13, also led to embryonic lethality around E10.5 (23). However, detailed characterization of the embryonic defects in *Gnas*$^{-/-}$ mice has not been reported.

In addition to defects in the embryos, homozygous *Snx13* mutants show striking defects in extra-embryonic tissues including the VYS endoderm and chorioallantoic placenta. VYS endoderm is an extra-embryonic cell layer of embryonic origin that plays important roles in nutrient uptake and transport (12). VYS endoderm cells have microvilli and contain a highly developed endocytic/lysosomal system, which allows efficient absorption and transport of nutrients from maternal sources to the fetus and degradation of maternal proteins in lysosomes to generate amino acids for protein synthesis in the fetus before the placenta taking over this function (11, 12, 14, 15). By electron microcopy and immunofluorescence we show that the endocytic/lysosomal compartments in the mutant VYS endoderm are dramatically altered compared with those of the wild-type VYS cells.

We consider that the defect in VYS endoderm is one of the most significant defects in *Snx13* mutants and may contribute, at least partially, to the other abnormalities observed. To begin with, growth retardation in the mutant embryos may be explained by the defects in nutrient uptake in VYS endoderm and maternal-fetal exchange. Second, defects in the uptake of small molecule nutrients such as vitamins in VYS endoderm may lead to neural tube closure defects in embryos (24, 25). Megalin, an endocytic receptor for multiple ligands including the vitamin B12–transcobalamin complex (26) and the retinol-binding protein–vitamin A complex (27), is localized at the apical surface of VYS endoderm during development (13). Cubilin, another receptor for the transport of vitamin B12, can also be found in VYS endoderm (13). Mice lacking megalin also showed defects in the forebrain (28). Furthermore, deficiency in vitamin B12 or retinoic acid has been shown to cause defects in neural tube closure in mice (25, 29). Finally, there is also a potential link between defects in the yolk sac and the chorioallan-

toic placenta. Placental hypoplasia with defective trophoblast differentiation and blood vessel development in the labyrinthine layer may result from a functional failure in vesicular transport of nutrients in VYS endoderm which is the primary structure responsible for the maintenance of the developing embryo and the formation of the chorioallantoic placenta before the establishment of the functional placenta. In the future it will be interesting to further examine the contribution of the extra-embryonic defects to the embryonic lethality and other features observed in *Snx13* mutants either by tetraploid aggregations or by breeding mice contains floxed alleles of *Snx13* ($Snx13^{F/F}$) with another group of mice that carry Cre recombinase under the control of an epiblast-specific promoter such as meox2 (30).

The abnormal endocytic/lysosomal compartmentalization in the VYS endoderm cells of *Snx13*-null mutants provides new insights into understanding the cellular function of RGS-PX1/SNX13 as a regulator of endocytic trafficking. Early endosomes contain two distinct domains, vesicular and tubular, which have been thought to be involved in receptor degradation and recycling pathways, respectively (2, 3). Tubular domains which are enriched for recycling receptors usually pinch off from the spherical core and form carriers for delivery to the cell surface. The unusual amount of these tubular structures observed in *Snx13*-null VYS endoderm cells might indicate a defect in the recycling pathway from early endosomes back to the apical cell surface or in trafficking through recycling endosomes in the pericentriolar region. This model is consistent with the finding that megalin distribution at the apical cell surface is much broader in mutant than in the wild-type cells. Megalin, a member of the low-density lipoprotein receptor family (31), dissociates from its ligands in early endosomes and normally returns to the plasma membrane via the recycling pathway (13, 21), and ARH escorts megalin throughout the endocytic pathway (21). The change in megalin and ARH localization in mutant cells indicates a shift in its distribution to the inside of the cell (presumably to recycling endosomes) and suggests defects in their recycling to the plasma membrane. The implication that RGS-PX1/SNX13 is involved in receptor recycling adds a new dimension to the role of RGS-PX1/SNX13 in receptor degradation previously demonstrated by using cultured cells and ectopic expression (10). Another striking feature in the *Snx13*-null VYS endoderm is the appearance of autophagic vacuoles which most likely reflects a deficiency in the supply of nutrients from endocytic uptake and/or lysosomal degradation in these cells, as autophagy represents a major cellular response to nutrient deprivation (18). We speculate that the presence of autophagic vacuoles may be secondary to the defects in receptor endocytosis and endosomal-lysosomal trafficking.

RGS-PX1/SNX13, together with RGS-PX2/SNX14 and RGS-PX3/SNX25, forms the subfamily G of mammalian RGS proteins (8). What distinguishes this subfamily from the rest of >25 different RGS proteins is the presence of PX domain, which can also be found in SNX proteins that regulate endocytic trafficking (5). Consistent with this unique feature, RGS-PX1 is the only RGS protein characterized so far that shows defects related to endocytic trafficking when mutated in mice.

Among the 29 SNX protein family members identified in mammals (5), SNX1 and SNX2 are the only ones for which gene-targeted mice have been reported (32). Whereas neither $Snx1^{-/-}$ or $Snx2^{-/-}$ mice show any obvious phenotypes, $Snx1^{-/-};Snx2^{-/-}$ mice die at mid-gestation, suggesting that SNX1 and SNX2 have redundant functions (32). Similar to $Snx13^{-/-}$ mice reported here, $Snx1^{-/-};Snx2^{-/-}$ mice also showed growth retardation, neural tube closure defects and abnormal morphology in apical VYS endoderm (32). However, there are distinct differences between the defects seen in the VYS endoderm. Unlike the tubular structures in $Snx13^{-/-}$ cells, increased amounts of apical globular dense structures were found in $Snx1^{-/-};Snx2^{-/-}$ VYS endoderm cells (32). These structures were labeled by acidic Lysotracker but did not appear to represent either early endosomes or mature lysosomes as judged by lack of immunostaining with EEA1, LAMP1 or LAMP2 antibodies. Also, no autophagy was reported. Moreover, in contrast to $Snx13^{-/-}$ VYS endoderm cells, the LAMP2 staining pattern in $Snx1^{-/-};Snx2^{-/-}$ VYS endoderm cells was the same as in the wild type (32). The fact that tubular structures were more abundant and lysosomes smaller in the $Snx13^{-/-}$ than in wild-type mice suggests a defect in the sorting or trafficking in endosomes. This possibility is consistent with the previously characterized role of RGS-PX1/SNX13 in the lysosomal degradation pathway (8). Thus, differences between the phenotype of VYS endoderm cells of $Snx1^{-/-};Snx2^{-/-}$ and $Snx13^{-/-}$ mice very likely reflect the involvement of these proteins in different steps of endocytic trafficking. Whereas RGS-PX1/SNX13 colocalizes with EEA1 and hepatocyte growth factor-regulated tyrosine kinase substrate (10), presumably on the clathrin-coated domains of early endosomes, SNX1 is localized on the tubular domains of endosomes, only partially overlaps with EEA1 staining, and plays a role in endosome-to-trans-Golgi network transport (7).

Taken together, our characterization of *Snx13* gene targeted mice has revealed essential roles for SNX13/RNS-PX1 in mouse development and the regulation of endocytosis dynamics in VYS endoderm cells. Furthermore, these studies provide new insights into the cellular function of RGS-PX1/SNX13 as a sorting nexin. In this study we focused on the role of RGS-PX1/SNX13 in the organization of endocytic compartments in VYS endoderm cells. Whether RGS-PX1/SNX13 plays a similar role in other cell types remains to be seen. Future experiments will be aimed at understanding the underlying molecular mechanisms involved by investigating the functions of RGS-PX1/SNX13 in adult mice by using the conditional knockout approach.

Materials and Methods

Construction of the Targeting Vector. A mouse 129/SvJ genomic library (Stratagene, La Jolla, CA) was screened by using a 5′ region of human RGS-PX1/SNX13 cDNA. Three independent clones expanding ≈20-kb region including coding exons 1 to 5 were isolated, subcloned into the pBluescript SKII vector and mapped for restriction enzyme sites. The targeting vector was constructed by using these genomic clones and the pflox vector which contains three *loxP* sites and a tk-neo selection cassette (33). A 2.0 kb SphI fragment containing coding exon 3 of *Snx13* was inserted into the BamHI site of pflox, which was flanked by two *loxP* sites, and adjacent *Snx13* genomic sequences were added by subcloning a 3.8-kb SphI fragment into the XhoI site and a 1.8-kb SphI-EcoRV fragment into the SalI site of pflox, respectively.

Electroporation and Selection of ES Cells. The NotI-linearized *Snx13* targeting construct was electroporated into R1 embryonic stem (ES) cells followed by G418 (Invitrogen, Carlsbad, CA) selection. Resistant clones were screened for homologous recombination by PCR with the upstream TK-specific primer and the downstream gene-specific primer. PCR positive clones were analyzed by Southern blotting with a 3′ external gene-specific probe to hybridize with KpnI-digested genomic DNA and a 5′ probe with BamHI-digested genomic DNA. The presence of three *loxP* sites was confirmed by using a *loxP* -specific probe. Representative ES cell clones containing a targeted allele were electroporated with a Cre expressing vector pCre-Hygro. Following selection with gancyclovir, subclones were isolated and analyzed by Southern blotting to identify Cre-mediated type I (deletion of both exon 2 and tk-neo, $Snx13^{\Delta}$ allele) and type II (deletion of tk-neo only, $Snx13^{F}$) mutants.

Generation of SNX13 Germ-Line Knockout Mice. Type I ES clones were microinjected into C57BL/6 blastocysts at the Moores Cancer Center transgenic mouse core facility at the University of California at San Diego. Male chimeric mice were mated with C57BL/6 females, and germ-line transmitted mice were bred with C57BL/6 mice for up to five generations to produce heterozygous mice. The

phenotypes reported were found in mice with a mixed background of 129Sv/J and C57BL/6.

PCR Genotyping. Genomic DNA from ES cells, visceral yolk sacs and tail biopsies were isolated by using DNeasy Tissue kit (Qiagen, Valencia, CA) and used for PCR analysis with Hotstar TaqDNA polymerase (Qiagen). Three primers were used to detect wild-type and null alleles: (5′ GCATTTCTGTGTGGTGTGTTTGTC 3′), (5′ CTGGTCTTGAACTTGCCTCCC 3′), (5′ CCAATAAGGACTGTATTCCATA GACC 3′), which produce 420- and 490-bp diagnostic fragments for wild-type and for $Snx13^{\Delta}$ alleles, respectively.

RT-PCR. RNA was prepared from E10.5 embryos by using an RNeasy kit (Qiagen). RT-PCR was performed by using the SuperScript Two-step RT-PCR system (Qiagen) according to the manufacturer's instructions. The primers used are: RT-1: (5′ ATGTTAACAGAGGCCAGTCTATCC 3′) which corresponds to the 3′ end of exon1, the 5′ end of exon 2 and RT-2 (5′ CTCATCAATT ATATTGGCACCCGTC 3′) which corresponds to the 3′ end of exon 4.

Histological Analysis. E8.5–13.5 embryos were derived from crossing of heterozygous mice. Noon of the day the vaginal plug was detected was defined as E0.5. Embryos and placentas were fixed overnight at 4°C in either 4% paraformaldehyde (PFA) in 0.1 M phosphate buffer, pH 7.2, or 10% neutral formalin. Samples were embedded in paraffin, sectioned, and stained with hematoxylin and eosin. Histology and immunohistochemistry were at the UCSD Moores Cancer Center Histology Core. The samples were examined by using a Zeiss Axiolab Microscope. Images were collected with a Sony Digital Camera DICC-500 by using Scion Image Version 1.60.

Whole-Mount CD31 Staining. CD31 staining was carried out as described in ref. 34. Embryos were fixed in 4% PFA in 0.1 M PBS, pH 7.3, at 4°C overnight and then dehydrated. Endogenous peroxidase activity was blocked by incubation in 5% H_2O_2 in MeOH. After blocking in PBSBT (3% skim milk, 0.1% Triton X-100 in PBS), the embryos were incubated overnight at 4°C with anti-CD31 IgG diluted 1:50 in PBSMT, washed 5 times over 1 h in PBSBT and incubated overnight at 4°C with an HRP-conjugated secondary antibody diluted 1:200 in PBSBT. After washing in PBSBT, color was developed by using a DAB kit (Vector Laboratories, Burlingome, CA) with 0.3 mg/ml DAB/0.5% $NiCl_2$/0.03% H_2O_2. Whole-mount embryos were photographed on a Leica MZ8 microscope.

Antibodies. Rabbit antibodies against the cytoplasmic tail of megalin (459) and ARH have been described in ref. 21. Rabbit antibodies against LAMP2 and LC3 were gifts from Ira Mellman (Yale University, New Haven, CT) and Takashi Ueno (Juntendo University, Tokyo, Japan), Respectively. Rat anti-CD31 (MEC13.3) was obtained from PharMingen. Cross-absorbed Alexa 488- or Alexa 594-conjugated goat anti-mouse or anti-rabbit $F(ab')_2$ were from Molecular Probes, and HRP-conjugated anti-rat antibodies from PharMingen.

Semithin Cryosections and Immunofluorescence Microscopy. Semithin cryosections were prepared and processed as described in refs. 21, 35, and 36. Briefly, VYS were fixed in 4% PFA in phosphate buffer followed by 15 min in 8% PFA, cryoprotected in sucrose and frozen in liquid nitrogen. Semithin cryosections (0.5–0.7 μm) were cut at −100°C with a Leica Ultracut UCT microtome equipped with an FCS cryoattachment. Samples were examined by using a Zeiss Axiophot microscope (Carl Zeiss, Thornwood, NY). Images were collected with an ORCA-ER camera (Hamamatsu, Bridgewater, NJ) by using Scion image version 1.59 (Scion, Frederick, MA) and processed by using Adobe Photoshop 5.5.

Electron Microscopy. VYS from E10.5–12.5 conceptuses were fixed in 1.5% glutaraldehyde, 3% PFA, 5% sucrose in 0.1 M cacodylate buffer, pH 7.4, at room temperature for 2 h. The samples were postfixed in 1% OsO4 in the same buffer for 1 h, stained *en-bloc* in 1% uranyl acetate in 10% ethanol for 1 h, dehydrated in ethanol and embedded in LX112. Semithin sections were stained with toluidine blue. Thin sections were stained with uranyl acetate and lead citrate and examined in a Jeol JEM 1200EX II electron microscope.

We thank the transgenic mouse and histology core facilities of the Moores Cancer Center, University of California at San Diego, for their assistance; Timo Meerloo for help with figure preparation; and Drs. Kurt Benirschke, Gordon Gill, Grace Zhao, and Yifeng Zhang for helpful discussions. This work was supported by National Institutes of Health Grants CA 100768 and DK 17780 (to M.G.F.). B.Z. was supported by an American Heart Association postdoctoral fellowship, and E.L. was supported by the University of Helsinki. T.T. and N.T. are members of the Molecular Pathology Graduate Program at the University of California at San Diego.

1. Gruenberg J (2001) *Nat Rev Mol Cell Biol* 2:721–730.
2. Mellman I (1996) *Annu Rev Cell Dev Biol* 12:575–625.
3. Mukherjee S, Ghosh RN, Maxfield FR (1997) *Physiol Rev* 77:759–803.
4. Worby CA, Dixon JE (2002) *Nat Rev Mol Cell Biol* 3:919–931.
5. Carlton J, Bujny M, Rutherford A, Cullen P (2005) *Traffic* 6:75–82.
6. Kurten RC, Cadena DL, Gill GN (1996) *Science* 272:1008–1010.
7. Carlton J, Bujny M, Peter BJ, Oorschot VM, Rutherford A, Mellor H, Klumperman J, McMahon HT, Cullen PJ (2004) *Curr Biol* 14:1791–1800.
8. Zheng B, Ma YC, Ostrom RS, Lavoie C, Gill GN, Insel PA, Huang XY, Farquhar MG (2001) *Science* 294:1939–1942.
9. Castellone MD, Teramoto H, Williams BO, Druey KM, Gutkind JS (2005) *Science* 310:1504–1510.
10. Zheng B, Lavoie C, Tang TD, Ma P, Meerloo T, Beas A, Farquhar MG (2004) *Mol Biol Cell* 15:5538–5550.
11. Copp AJ (1995) *Trends Genet* 11:87–93.
12. Bielinska M, Narita N, Wilson DB (1999) *Int J Dev Biol* 43:183–205.
13. Christensen EI, Birn H (2002) *Nat Rev Mol Cell Biol* 3:256–266.
14. Lloyd JB (1990) *Teratology* 41:383–393.
15. Jollie WP (1990) *Teratology* 41:361–381.
16. Christensen EI, Birn H, Verroust P, Moestrup SK (1998) *Int Rev Cytol* 180:237–284.
17. Lou X, McQuistan T, Orlando RA, Farquhar MG (2002) *J Am Soc Nephrol* 13:918–927.
18. Levine B, Klionsky DJ (2004) *Dev Cell* 6:463–477.
19. Farquhar MG (1995) *J Clin Invest* 96:1184.
20. Rodman JS, Kerjaschki D, Merisko E, Farquhar MG (1984) *J Cell Biol* 98:1630–1636.
21. Nagai M, Meerloo T, Takeda T, Farquhar MG (2003) *Mol Biol Cell* 14:4984–4996.
22. Tanida I, Ueno T, Kominami E (2004) *Int J Biochem Cell Biol* 36:2503–2518.
23. Yu S, Yu D, Lee E, Eckhaus M, Lee R, Corria Z, Accili D, Westphal H, Weinstein LS (1998) *Proc Natl Acad Sci USA* 95:8715–8720.
24. Copp AJ, Greene ND, Murdoch JN (2003) *Nat Rev Genet* 4:784–793.
25. Ray JG, Blom HJ (2003) *Q J Med* 96:289–295.
26. Moestrup SK, Birn H, Fischer PB, Petersen CM, Verroust PJ, Sim RB, Christensen EI, Nexo E (1996) *Proc Natl Acad Sci USA* 93:8612–8617.
27. Christensen EI, Moskaug JO, Vorum H, Jacobsen C, Gundersen TE, Nykjaer A, Blomhoff R, Willnow TE, Moestrup SK (1999) *J Am Soc Nephrol* 10:685–695.
28. Willnow TE, Hilpert J, Armstrong SA, Rohlmann A, Hammer RE, Burns DK, Herz J (1996) *Proc Natl Acad Sci USA* 93:8460–8464.
29. Bavik C, Ward SJ, Chambon P (1996) *Proc Natl Acad Sci USA* 93:3110–3114.
30. Tallquist MD, Soriano P (2000) *Genesis* 26:113–115.
31. Saito A, Pietromonaco S, Loo AK, Farquhar MG (1994) *Proc Natl Acad Sci USA* 91:9725–9729.
32. Schwarz DG, Griffin CT, Schneider EA, Yee D, Magnuson T (2002) *Mol Biol Cell* 13:3588–3600.
33. Priatel JJ, Sarkar M, Schachter H, Marth JD (1997) *Glycobiology* 7:45–56.
34. Ryan HE, Lo J, Johnson RS (1998) *EMBO J* 17:3005–3015.
35. McCaffery JM, Farquhar MG (1995) *Methods Enzymol* 257:259–279.
36. Lehtonen S, Lehtonen E, Kudlicka K, Holthofer H, Farquhar MG (2004) *Am J Pathol* 165:923–936.